A three-dimensional study of the glottal jet

Florian Krebs, Fabrice Silva, Denisse Sciamarella, Guillermo Artana

Noname manuscript No.
(will be inserted by the editor)

A Three-dimensional Study of the Glottal Jet

F. Krebs · F. Silva · D. Sciamarella · G. Artana

Received: date / Accepted: date

Abstract This work builds upon the efforts to characterize the three-dimensional features of the glottal jet during vocal fold vibration. The study uses a Stereoscopic Particle Image Velocimetry setup on a self-oscillating physical model of the vocal folds with a uniform vocal tract. Time averages are documented and compared against observations reported for jets exiting elongated nozzles. Phase averages are locked to the audio signal and used to obtain a volumetric reconstruction of the jet. From this reconstruction, the intra-cycle dynamics of the jet axis switching is disclosed.

Keywords glottal jet · 3D PIV · vocal folds · axis switching

1 Introduction

Recently, there have been many studies attempting to assess the dynamics and topology of the fluid dynamical processes taking place in the larynx during vocal fold oscillation. Research in the field has the purpose of gaining insight into the underlying physics of this biological flow, and of understanding the interplay between the flow dynamics and the structures in the larynx. With the exception of a few specific cases in which this biological flow can be studied as

F. Krebs · F. Silva · G. Artana
LFD, Facultad de Ingeniería
Universidad de Buenos Aires - CONICET
Av. Paseo Colón 850, C1063ACV Buenos Aires, Argentina
Tel.: +54-11-43430092
Fax: +54-11-43311852
E-mail: gartana@fi.uba.ar

D. Sciamarella
CNRS, Bâtiment 508,
Université Paris-Sud, 91403 Orsay, France
E-mail: denisse@limsi.fr

being mainly two-dimensional [5,30], most investigations concur on the existence of highly three-dimensional features for the glottal jet (see Table 1). So far, characterizations of three-dimensional features of the glottal jet have been performed with classical (two-dimensional) Particle Image Velocimetry (2D-PIV), a technique which provides the projection of the velocity vector into a flow slice. The study presented in this work is three-dimensional because it uses Stereoscopic Particle Image Velocimetry (SPIV), a method providing the complete set of velocity components in a flow slice. For highly three-dimensional flows, SPIV is expected to determine the in-plane components with a greater accuracy than 2D-PIV [26]. For cyclic flows, synchronizing the acquisition of SPIV data at different slice positions permits a volumetric reconstruction of the flow development. Achieving this kind of reconstruction for quasi-cyclic flows is not always possible, depending on the type of flow under study and on the synchronisation method.

Glottal flow is the quasi-cyclic airflow generated during voice production. The flow is expelled from the lungs, and passes through the glottis, the aperture delimited by the vocal folds. The vocal folds are two bands of muscle tissue capable of sustaining flow-induced oscillations, with either an incomplete or a complete closure of the glottis. In the latter case, there is a phase of the glottal cycle during which airflow is interrupted. A diagram illustrating the glottal jet and vocal fold motion in a typical glottal cycle is given in Fig 1. Glottal flow typically presents a certain inter-cycle variability. There are numerous factors that may alter the fluid-dynamical cycle, as has been shown with the observation of glottal jet flapping, or asymmetric flow separation. In fact, glottal jet formation at the vocal folds and vocal fold motion are the common result of a fluid-structure interaction process which has been recognized to be highly dependent on flow separation [23]. Numerical studies have shown that flow separation mobility in the glottis cannot be reduced, in general, to a function of the glottal geometry [29]. A study of the features of the glottal jet must therefore face the complexity implied by the non trivial physics of jet formation at the moving folds - see for instance [8]. It is the scope of this work to overcome the difficulties related to the volumetric reconstruction of the dynamics of a jet generated by a self-oscillating valve mimicking vocal fold behavior, and to analyze the reconstructed jet on the basis of observations reported for jets exiting elongated nozzles.

The diversity in vocal fold models, configurations and settings used in glottal jet studies is quite large. For different experimental reasons, some works used mechanical or *ex vivo* prototypes, water rather than air as a working fluid, and/or externally driven rather than self-oscillating models. A survey of this assortment is provided in the table dressed by Triep and Brucker in [33]. Velocity field measurements in upscaled water experiments allow for lower velocities and frequencies, but experiments in air have the advantage of an acoustic output which can be recorded along with the velocity fields. Driven vocal fold models allow for a direct control over the behavior of the structure, but only self-oscillating models reproduce the energy balance between fluid, structure and sound. Table 1 presents a summary of the main observa-

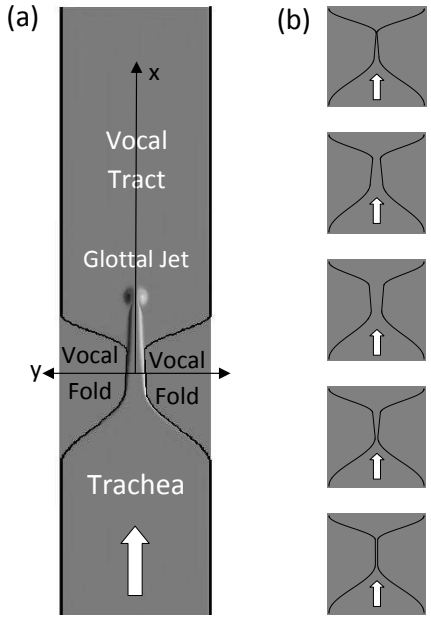

Fig. 1: Schematic diagram of the glottal jet (a) and a of a cycle of vocal fold motion (b). The cycle starts at the top with vocal fold opening and ends at the bottom with vocal fold closure. Airflow direction is indicated with a white arrow.

tions reported in 2D-PIV glottal jet studies, regardless of the divergence in experimental choices.

In contrast to certain flow features which appear to be case-dependent, Table 1 shows that jet axis switching is a three-dimensional effect which extends over the variety of experimental setups. For jets exiting non circular orifices, axis switching can be defined as a particular evolution of the cross section of a jet, such that the jet axes appear as succesively rotated at angles which are characteristic of the jet geometry. From the literature review on non circular jets proposed by Gutmark and Grinstein [11], jet axis switching is known to depend on many parameters, such as Reynolds number, initial shear-layer thickness distribution, nozzle geometry and aspect ratio. Some processes, such as small-scale vorticity production, are exclusive to the existence of sharp corners. The case of jet axis switching in glottal-like flow is particularly complex because real vocal folds define an orifice with an elongated geometry that has sharp corners and a cyclic motion implying time-varying aspect ratio and Reynolds number. It is therefore of interest to consider a laboratory jet flow that reproduces these features. This makes the choice of the vocal fold prototype particularly important.

2D-PIV	Flow Separation	Jet Flap	Starting Vortices	Shear-layer Vortices	Vena Contracta	Axis Switch
Triep [34,33]	S	no	yes	A	MS	yes
Krane [18]	S	-	yes	S	MC	-
Neubauer [22]	-	yes	A	S	-	yes
Khosla [15,16]	A	yes	A	S	-	yes
Drechsel [6]	IG	FJ	S	S	-	yes
Becker [2]	A	-	-	-	-	-
Erath [7]	A	-	-	-	-	-
Sidlof [30]	IG	-	-	-	-	-

Table 1: Main observations reported in studies of glottal flow with 2D-PIV techniques. Only the name of the first author is given. The dash symbol means that there is no reference to the corresponding feature in the article. Jet Flap refers to flapping due to downstream large-scale vortices. Axis switch reports are all inferred from the observation of a mid-sagittal narrowing of jet flow. Labels denote: A-asymmetric (unsteady Coanda), S-symmetric, MC-Midcoronal, MS-Midsagital, IG-Intraglottal, FJ-In free jet case.

The vocal fold valve used in this work is based on the design developed in Ruty *et al* [28,27], which consists of a pair of thin latex lobes filled with water under pressure. The self-sustained oscillations of this model define, during the open phase, an outlet presenting the shape of an elongated orifice, with time-varying aspect ratio and sharp corners at the commissures. The design also reproduces the generation of a strong tonal acoustic signal and the possibility of controlling the natural frequency of the artificial folds as a dynamical control parameter. The model can be used either in free jet experiments or attached to a duct representing the vocal tract. While free jet experiments are useful to evaluate the *in vacuo* performance of a vocal fold model, an assessment of the flow confinement effects acted by the vocal tract is certainly relevant. The configuration adopted for the SPIV measurements includes the vocal tract, not only because it makes part of the conditions encountered in human phonation, but also for technical reasons. The presence of the tract assures an important number of resident seeding particles in the region of interest, thus facilitating flow velocimetry with PIV. As previous research works indicate that the region of major interest from the point of view of sound production lies in the vicinity of the flow discharge [37], the SPIV measurements of the present study are conducted as close as possible to the valve exit.

The article is organized as follows. Section 2.3 describes the full experimental setup and the methods implemented for data analysis. Section 3 presents the results, which include instantaneous velocity fields, velocity profiles from time and phase averages along the minor and major axes, the volumetric reconstruction of the jet and the characterization of the axis switching dynamics. Section 4 presents concluding remarks related to the reported observations.

2 Materials and methods

2.1 Arrangement of the Experimental Setup

Fig 2 shows the general arrangement of the SPIV experimental setup. Compressed air was supplied by a laboratory network and adjusted with a pressure regulator. The mean airflow was monitored with a floating-ball flowmeter and seeded with smoke particles. The phonatory system was represented with three elements: a circular pipe at the place of the trachea fed by the pneumatic system, the water-filled valve representing the vocal folds, and a square-section transparent duct playing the role of a uniform vocal tract without false vocal folds. The height of a water column determined the water pressure inside the artificial folds. A variation of the height of the water column translates into a variation of the natural frequency of the valve – [28,27]. The laser optics in front of the double-pulsed laser formed the light sheet illuminating the flow in the area of interest. An omnidirectional measurement condenser microphone captured the sound pressure emitted by the system. The microphone was placed close to the tract exit without interfering with the flow. The arrangement of the cameras shown in the figure corresponds to the one used in the SPIV experiments. This arrangement was conveniently changed for high-speed imaging of the valve motion.

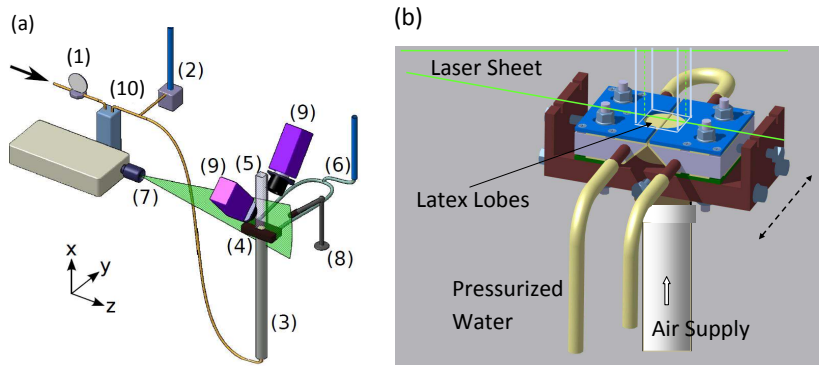

Fig. 2: (a) Schematic diagram (color online) of the general experimental arrangement with (1) flow meter, (2) air pressure control, (3) upstream pipe, (4) vocal fold model, (5) downstream duct representing vocal tract, (6) water pressure control, (7) laser and light sheet, (8) microphone, (9) cameras arrangement for SPIV measurements, (10) air supply and seeding system. (b) Enlarged view of the vocal fold valve.

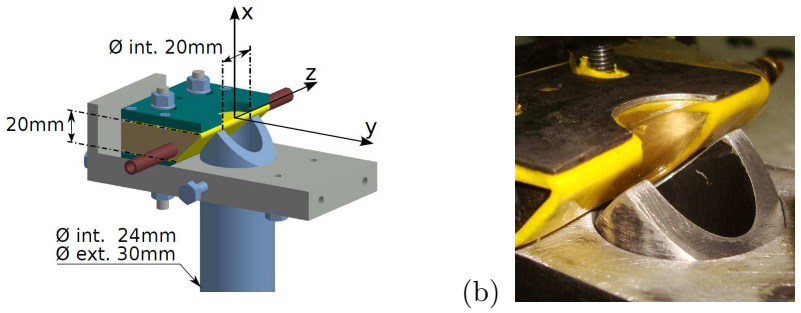

Fig. 3: Vocal fold valve mounting process. (a) Broken view of the support of the artificial folds with the upstream pipe; (b) Detail of the latex lobe mounted in the support before water-filling.

2.2 Vocal Fold Model characteristics

A first water filled design of vibrating folds was introduced by Gilbert *et al* [10] with the goal of studying the buzzing lips of the trombonist (see also [35]). The same type of valve was later adapted by Ruty *et al* [28,27] to study the human vocal folds. The valve used in this work is inspired in Ruty's model. It consists of a metallic support over which a couple of covers made of a deformable material can be laid and adjusted, to be filled with water – see Fig 3 (a) and (b). Fold oscillations are excited when the air flows through the water-filled folds above a certain threshold air pressure. The advantage of this model is that a dynamical variation of the fundamental frequency can be obtained by adjusting the water pressure: the valve is thus both self-oscillating and tunable.

In the experiments presented in this work, covers were made of 0.05 mm-thick latex. Once the covers were set face-to-face, they were filled with water under pressure to form the replica of the vocal fold pair. Valve functioning can depend on the pre-stress applied on the latex during the mounting procedure. For this reason, the valve was mounted once and remain unchanged during all the velocimetry experiment. At the water pressure used in the experiments, there was no pre-oscillatory gap between the latex folds. When vibrating, the artificial folds defined an aperture with a time-varying cross section. The glottal width in the experiments ranged from zero (complete closure) to approximately 2 *mm*. Air supply was controlled by the pneumatic system, ending in the 80 *cm*-long pipe representing the trachea. This pipe had an internal diameter of 24 mm and an external diameter of 30 mm. Near the valve support, there was a continuous transition of about 5° which ended up in an inner diameter of 20 mm. On top of the vocal fold model, a square-section transparent duct (20 mm× 20 mm× 17 cm) could be attached (detached) depending on whether the vocal tract was considered (or not) as part of the system.

To capture fold motion, a high-speed camera (512×512 pixels resolution, 2500 fps maximum, $1\mu s$ shutter minimum) was placed downstream in the jet axis. An account of the valve oscillation modes that may be excited without a vocal tract was provided in [19].

2.3 Flow Velocimetry Devices

In the experiments presented in this article seeding particles were generated by joss sticks. This kind of seeding did not interfere with valve functioning and proved to be more adequate than other tested alternatives (oil sprays having a mean particle size lower than 2 μm, or cigarette smoke). Joss stick tracers yielded finer-grained images compatible with the PIV processing purposes. An exhaust hood placed 1 m away from the test area and operated at a low velocity prevented the room from smoke filling. Maximum Stokes number (Sto) of the seeding particles is given by τ_p/τ_f, where τ_p and τ_f are the particle and flow time scales respectively. The value of $\tau_p \sim 3$ μs is computed as $\rho_p D_p^2/18\mu_0$, with $\rho_p \sim 10^3$ kg/m^3 the particle density, $D_p \sim 1$ μm the particle diameter and $\mu_0 = 18.27\mu$Pa s the air viscosity [9]. Following [21], the value of τ_f can be obtained from δ/U_{CL}, where $\delta \sim 2$ mm is the shear layer thickness obtained from vorticity field inspection, and $U_{CL} \sim 30$ m/s is the local streamwise centerline velocity. This yields $\tau_f \sim 67$ μs and then, $Sto \sim 0.04$, which is lower than the 0.2 value typically demanded for flow visualization in incompressible flows – see for instance [4].

For velocimetry measurements, the laser was set at full power and images were processed with a commercial software. The working distance of the cameras was about 30 cm. In order to avoid damage of pixels because of excessive light incidence upon the CCD, the laser reflections from the vocal fold model had to be eliminated. Reflections from the metallic support were suppressed with antireflection paint, while reflections from the artificial folds (which could not be painted) were suppressed by interposing small pressboard visual screens between the cameras and the folds. These screens impeded acquiring images of the close vicinity of the valve exit. The first available measurement points lay about 6 mm away from the $x-$axis origin (located as indicated in Fig 3a).

All SPIV measurements were undertaken with the full system: cylindrical pipe + valve + duct. Attaching the square-section duct served the double purpose of representing the vocal tract and of assuring a sufficient number of resident seeding particles in the whole field of view and during the complete cycle. The double-pulsed laser light sheet (thickness $\sim$ 1.5 mm) made the tracer visible in a defined slice of the flow field. The motion of the tracer particles was captured at two consecutive instants (two 8 ns-long pulses within 3 μs) by a calibrated arrangement of two triggered cameras (1648×1214 pixels resolution, 14 -bit digital output, 30 fps maximum, 110 ns minimum inter-frame time, with Scheimpflug adapters). The three components of the velocity field were computed from the displacement of the particles projected on the two non-parallel camera planes (four images). The model was mounted in

a moving platform that enabled capturing flow slices at different locations and/or with different orientations, without involving new optical alignements, focusing or calibrations. The platform was translated sequentially to obtain a series of coronal (x-y) slices for a subsequent volumetric reconstruction of the flow. Fine screw drives offered fine resolution positions with an accuracy of 0.1 mm.

The SPIV system measures the out-of-plane velocity together with the in-plane velocities. The commercial system used in the experiment enabled a self-calibration of the device for this purpose. For a camera angle α, the out-of-plane error is predicted to be a factor $1/tan(\alpha)$ of the in-plane components. For the camera arrangements of the SPIV experiment, α was close to 45°, so that the out-of-plane error is of the same order as the in-plane error. In a very penalizing estimation, the latter error can be calculated with the inter-frame time and a quarter of pixel displacement (about 1 m/s). Since the two cameras contribute equally to the final result, the absolute value of the in-plane error is smaller (by $1/\sqrt{2}$) than the corresponding value for a single camera arrangement. The stereo arrangement also removes perspective errors which can be quite sizable in single camera PIV unless telecentric lenses are used [24,17]. When the cameras are placed on either side of the light sheet, the included angle is not constant across the field of view and hence, the measurement uncertainty for the out-of-plane component is not constant. For the rather narrow field of view in this study (5°), this variation was of no significance.

2.4 Post-synchronisation of data sets

The parameters of the PIV data evaluation were set as follows. The correlation method used cross-correlation, multi-step, decreasing size; the size of the interrogation window was 64×64 (1 pass) and 32×32 (2 passes); the window weight was circular; the overlap was 50 % and the post-processing used a median filter (remove and replace, fill up empty spaces).

Workstation's transfer time, laser's repetition rate and limited camera cache memory restricted the maximal sampling rate of the SPIV system to 5 Hz, a frequency that is about ten times lower than the fundamental frequency at which the valve oscillates in the experiment. Because the SPIV acquisition of multiple samples within a single oscillation cycle was impossible with this setup, a post-synchronisation of the acquired data sets was implemented. The post-synchronisation method assumes that the fundamental periods of the three acquired data sets (sound, valve motion and emerging flow) are correlated. In other words, if there are variations in the fundamental period of the acoustic signal, the cycles corresponding to valve motion and emerging flow will vary accordingly in the same way.

PIV systems generally enable to trigger image acquisition with an external signal to undertake phase-locked PIV data analysis. Nevertheless, because the audio signal generated by the self-oscillating system presented small variations

in the fundamental frequency, the use of an external trigger was likely to introduce errors in an real-time phase determination. To avoid this difficulty, both the audio signal and the instants corresponding to the internal trigger of the SPIV system (set to 5 Hz) were simultaneously recorded all along the experiments. In a single experiment and for each slice position, 1000 images were acquired. Data acquisition lasted 200 seconds per slice, during which about 11000 audio cycles were recorded.

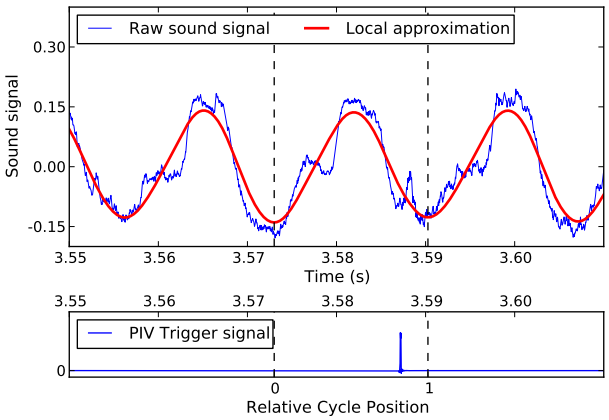

Fig. 4: Example of the audio signal obtained during the SPIV experiment and processed for post-synchronisation, based on the determination of a Relative Cycle Position (RCP). (Color online)

The post-processing of the data was used to determine, to which portion of a certain cycle of the sound signal one should attribute an acquired flow image, despite a possible non negligible inter-cycle variability. After the experiment, a local analysis of the sound signal was performed in the vicinity of every trigger. An interval of 6 cycles centered around the trigger was inspected. Within the interval, the audio signal was filtered with a zero phase Butterworth bandpass filter of order 2 with cut-off frequencies of 40 Hz and 80 Hz. The local period was computed from the two minima of the locally filtered signal that enclose the trigger instant. The relative cycle position (hereafter denoted RCP) of a snapshot of the flow field was defined as the elapsed time between the associated SPIV system trigger instant and the closest anterior minima, normalized by the computed local period – see Fig 4. To this end, we use an approximation of the quasi-harmonic filtered signal based on a high order expansion on first kind Chebyshev polynomials. In this manner, the RCP was well determined for a given snapshot.

3 Results

3.1 Operating conditions

The artificial folds used in this work present oscillation ranges which do not exactly coincide with physiological ranges. According to [13], human vocal folds have an oscillation range of $78 - 1108$ Hz. The artificial folds can phonate in a wide range of frequencies, and particularly, at frequencies below the inferior limit of the human oscillation range (~ 50 Hz). For some parameter values, the longitudinal behavior of the valve shows irregular oscillations [19]. By irregular oscillations it is meant that the valve can vibrate with visible asymmetries with respect to the line joining the anterior-posterior commisures of the folds, or with a glottal orifice that splits into separate areas during the cycle. The operation conditions of the vocal fold model were chosen to obtain regular vibrations in this sense, since this is the type of structural behavior that is encountered in normal phonation [31].

Fig 5 shows a sequence of top views of the high speed images of the artificial folds sustaining self-oscillations. The open exit area of the valve varied from an opening to a fully closed position. During the open phase –frames (a) to (i)– the apparent glottal length increased and decreased during the opening and closing phases respectively. The time evolution of the glottal orifice in this configuration is consistent with a typical maximum glottal width of about 2 mm. The closed phase –frames (j), (k), (l)– corresponds to a quarter cycle.

Section 3.2 shows the results of the SPIV measurements performed with a vocal tract attached, a fundamental frequency $f_0 \sim 55$ Hz, a mean subglottal overpressure of 15 $cm\ H_2O$ and a mean flow rate of $5.5 \times 10^{-4}\ m^3/s$. For a Reynolds number based on the channel's height and the maximum flow rate, this corresponds to a maximum Reynolds of 2600. These settings clearly fulfilled the regularity condition mentioned above. As argued by Becker *et al* [2] – who worked farther below the inferior limit of the phonational range – the fact that the artificial fold system produces a clear tonal component in the acoustic signal suggests that the main physical processes responsible for voice production are being reproduced.

The acoustic signal can be used to characterize the response of the valve during the SPIV measurement. There is one audio signal per slice during the SPIV experiment. Jitter was evaluated using the Praat software (v5.1.29) as described in [3], with waveform matching pitch-mark detection [32]. The so-called *local jitter* (measuring cycle to cycle variability of pitch period) was 0.76% for the whole experiment. This value is consistent with a nonpathological voice discrimation (i.e. below 1.04%). Similarly, *local shimmer* (measuring cycle to cycle variability of amplitude) was estimated to 1.01 dB.

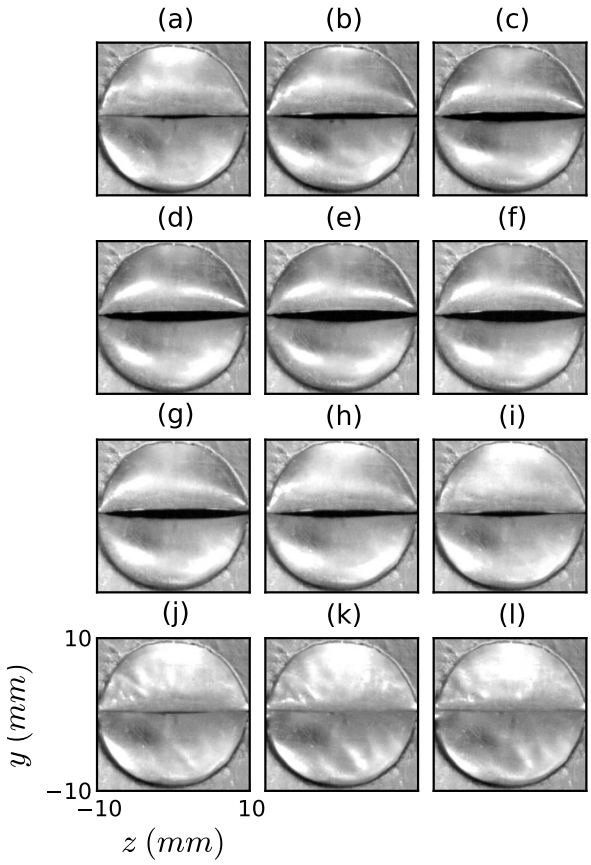

Fig. 5: Sequence of top views of the high speed images of the valve without a vocal tract. Regularly spaced snapshots along a single oscillation cycle.

3.2 SPIV captured Velocity Fields (with vocal tract)

This section contains representative results of the SPIV measurements before volumetric reconstruction. All the velocity fields correspond to flow measurements in the jet developing region ($x \geq 6$ mm) for the system with the vocal tract attached. Because of the technical constraints mentioned in section 2.3, the laminar core region is out of the field of view. Lower case v is reserved for instantaneous velocity fields, $\langle v \rangle$ denotes time averages and upper case V is used for phase averages.

3.2.1 Instantaneous flow fields

Fig 6 presents three instantaneous velocity fields $v(x, y, z)$ corresponding to approximately the same relative cycle position for different cycles during a

single experiment, without any variation of the control parameters. The three snapshots correspond to the same slice in space. The samples are chosen to illustrate the kind of inter-cycle variability encountered in the fluid dynamical cycle of this glottal jet. The diversity of flow fields is compatible with the complex fluid-structure interaction that generates the flow. The differences between the three snapshots are apparent: the first snapshot shows a jet with a spread rate that is approximately linear, in contrast with the second and third snapshots where the jet structure seems to be compatible with the starting and shear-layer vortices of Table 1 and of Fig **??**B. The second snapshot differs from the third one in the skewing of the jet axis. When jet axis skewing occurs, it is difficult to decide if the cause is a slight asymmetry in fold oscillation, or an asymmetry in flow separation from the folds (unsteady Coanda effect). For a quantification of the inter-cycle variability, the reader is referred to Fig 11.

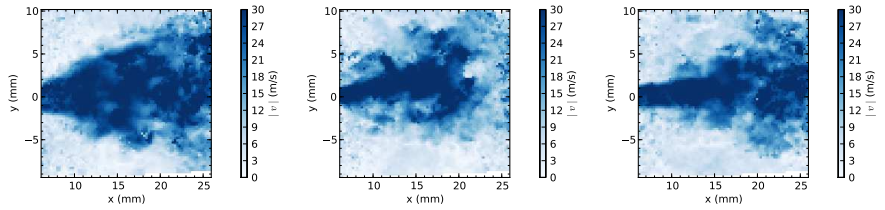

Fig. 6: Snapshots of the absolute value of the velocity collected at a constant plane ($z = 0mm$) and at approximately the same Relative Cycle Position (within the range $RCP = [0.898, 0.902]$) throughout a single experiment with vocal tract. (Color online)

3.2.2 Time-Averaged flow fields

This section presents time-averaged quantities calculated from the mean of all the instantaneous velocity fields captured per slice throughout the SPIV experiment. Since the study deals with a highly unsteady interrupted flow through a closing valve, the mean fields cannot be interpreted as stationary magnitudes to which small fluctuations are superposed. However, mean fields remain significant for characterization purposes because they usually condense salient features of the flow under study.

Documenting time averages also serves the purpose of comparing the investigated flow with results of related studies. The case study that is chosen as reference is Murugappan *et al* (2008)[21] for two reasons. Firstly, the nozzle in [21] presents some similarities with the valve used in the present work: the generated jet emanated from an elongated self-oscillating nozzle opening and closing along a cycle. Secondly, the study is quite recent and relates time averaged measurements with the data available from the literature on flow through non-circular nozzles. The time-averaged quantities considered in [21]

are jet spread, centerline velocity decay and velocity profiles. In order to show these quantities in juxtaposition with the current results, an equivalent nozzle diameter is introduced. The equivalent diameter for high aspect ratio nozzles is often defined as the diameter of a circular jet with momentum flux equal to that of the elongated jet – see for instance [14]. This length scale, which is easy to define in experiments concerning static nozzles, remains somewhat arbitrary for the folds in motion of the current study. The definition adopted here follows [21]: the average area of all the open phases is used to calculate an average open equivalent diameter D_e, of 4 mm in the current study.

Fig 7 presents the time-averaged jet spread, quantified by the half widths in the minor and major axes (respectively labeled $\overline{\Delta y}$ and $\overline{\Delta z}$) at different streamwise locations . The minor axis plane is the mid-coronal plane (xy), and the major axis plane is the mid-sagittal plane (xz). The magnitudes $\overline{\Delta y}$ and $\overline{\Delta z}$ are computed as the half widths of the 2D gaussian profiles that best fit the experimental values of $\langle v_x \rangle$ for each x position. The mean jet spread in the mid-coronal plane presents a linear expansion that contrasts with the contraction-expansion observed in the mid-sagittal plane. With the exception of the x-value at which $\overline{\Delta y}$ and $\overline{\Delta z}$ intersect, the mean flow has a cross section that is elongated, with an orientation that switches at the intersection point. This is the signature left in the mean field of the axis switching phenomenon, the most salient three-dimensional feature of this flow. The intra-cycle dynamics of this effect is discussed in detail in terms of phase averaged results, but its influence on the flow is already captured by the time-averaged field.

The jet flow field in the reference study presents two different modes depending on the tension applied to the flexible nozzle and the volumetric flow through it: the nonflapping mode (cases 1 and 2) and the flapping mode (cases 3 and 5). In the nonflapping mode, the jet has a straight centerline, while in the flapping mode the centerline steers from one side to the other. The mean jet spread in the minor axis ($\overline{\Delta y}$) of the present study is encompassed by the nonflapping cases of the reference work. This is in agreement with the typical instantaneous velocity fields presented in the previous section. The glottal jet centerline may be skewed (as in the second snapshot of Fig 6) but it does not zigzag, at least in the inspected region.

The jet spread in the major axis ($\overline{\Delta z}$) is not documented in the reference work, nor in the pulsating jet studies that the reference work quotes for comparison. However, a jet spread along the major axis with the trend observed in the current study is typical of axis-switching jets emanating from elongated nozzles. Among the non-circular steady cases revisited in [21], the elliptic jet studied in [36] and [12] present a jet spread that successively contracts and expands as the distance from the nozzle increases.

For steady jets, the local centerline mean velocity along the streamwise direction is known to be highly dependent on orifice geometry, especially for nozzles of aspect ratio less than or equal to ten [20]. Fig 8 shows $< v_{CL} >$ versus x/D_e for the glottal jet, juxtaposed with the values reported in [21] for flapping and nonflapping cases. In the plot, data have been normalized using a reference velocity $< v_{Ref} >$ defined as the local mean centerline velocity

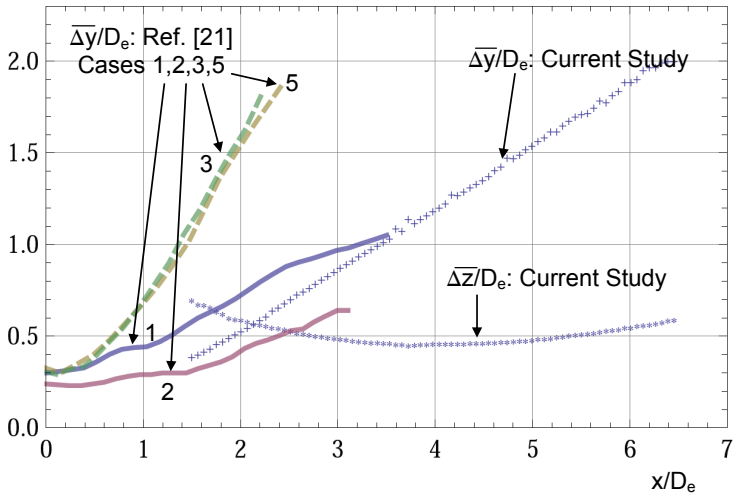

Fig. 7: Normalized jet half-widths $\overline{\Delta y}$ and $\overline{\Delta z}$ in the minor and major axes (y and z) versus x. Lines are used for results in [21] for $\overline{\Delta y}$ (results for $\overline{\Delta z}$ are unavailable): full lines are reserved for cases with no flapping, and dashed lines for cases with flapping. (Color online)

at the most upstream x value that was available for SPIV measurement. The reference work and the current study differ, not only in the design and operating conditions of the nozzle, but also in the inspected range of streamwise locations. In the x/D_e interval that is common to both studies, the centerline velocity curves have neighboring values but do not decay in the same manner. In fact, the glottal jet presents a slowly increasing acceleration of the decay, that has been reported for some steady elliptic jets, namely [12, 25].

Fig 9 presents the normalized mean velocity profiles $\langle v_x \rangle$ and $\langle v_y \rangle$ in the mid-coronal plane (dependence on $y/\overline{\Delta y}$ at different x/D_e locations). The adopted normalization makes the $\langle v_x \rangle$ profiles collapse on almost the same curve for $x/D_e > 2.5$. The $\langle v_y \rangle$ profiles do not collapse onto a single curve, but they retain a shape that is similar across the inspected x/D_e values, and the peak values of the profiles increase gradually as x/D_e grows. This suggests the possibility of a similarity analysis for the velocity profiles of the glottal jet, comparable to the analysis done for synthetic jets in [1], an issue that will be adressed in a separate paper. As in [21], only positive values of y are shown, but the reader should beware that $\langle v_x \rangle$ and $\langle v_y \rangle$ are respectively approximated by even and odd functions of $y/\overline{\Delta y}$.

In contrast to what is found in the current study, $\langle v_x \rangle$ and $\langle v_y \rangle$ in [21] present a variety of profile shapes which is much less regular: for $\langle v_x \rangle$, the profile waveform changes from case to case, and for $\langle v_y \rangle$ profiles differ in shape for different x/D_e locations within a single case. For the sake of clarity, a few reference profiles are represented in juxtaposition with the data of the present

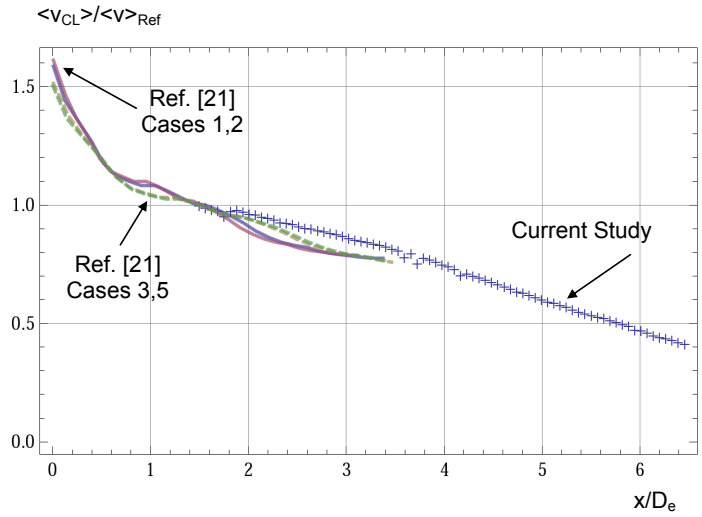

Fig. 8: Centerline velocity as a function of the normalized streamwise direction (x/D_e). Results in [21] are plotted for comparison. (Color online)

study. The differences between the profile shapes of the current study and those of the reference work can be attributed to experimental settings which differ, not only in flow rate, fundamental frequency or valve behavior, but also in the boundary conditions (the jet in [21] is free while the glottal jet of the SPIV measurements is laterally confined).

Fig 10 contains the normalized mean velocity profiles $\langle v_x \rangle$ and $\langle v_z \rangle$ in the mid-sagittal plane (dependence on $z/\overline{\Delta z}$ at different x/D_e locations). Equivalent results in [21] are not available. As functions of $z/\overline{\Delta z}$, $\langle v_x \rangle$ and $\langle v_z \rangle$ are respectively even and odd. The reflection symmetry with respect to the vertical axis of the plots is not perfect, but slightly lateralized mean profiles are frequent in confined flows. Replicating the trends found in the mid-coronal plane, the mid-sagittal plane shows $\langle v_x \rangle$ profiles collapsing onto a single curve, and $\langle v_z \rangle$ profiles exhibiting a gradual variation of the peak values of the profiles as x/D_e increases.

3.2.3 Phase averaged flow fields

To construct the phase averaged flow fields, the glottal cycle has been partitioned into 36 subdivisions or phases, labeled φ. An offset value of 0.5 is introduced with respect to the RCP scale, so that the opening phase of the valve occurs at the phase origin $\varphi = 0$. With 1000 acquisitions per slice in a single experiment, the number of images available in the mean per slice and per phase is 28. This is the number of realizations used to compute each phase averaged velocity field $V_\varphi(x, y, z)$.

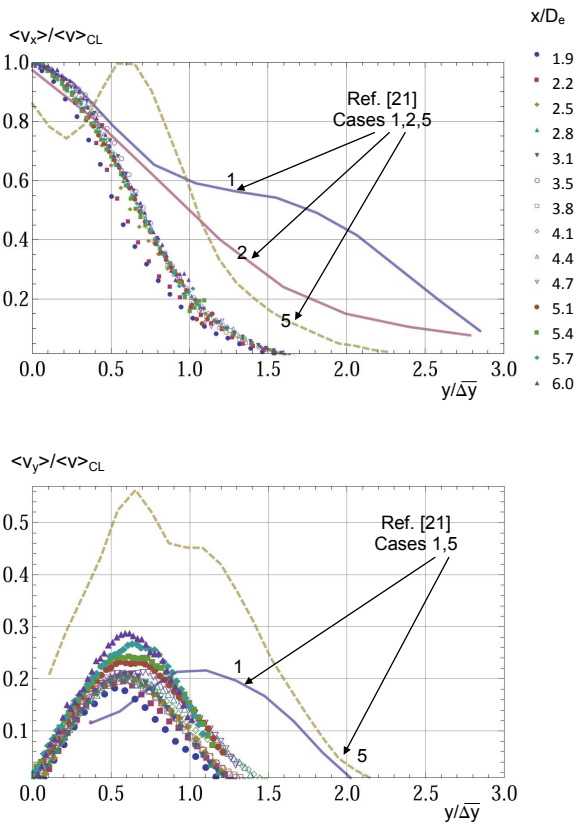

Fig. 9: Normalized mean velocity profiles $\langle v_x \rangle$ and $\langle v_y \rangle$ in the mid-coronal plane (dependence on $y/\overline{\Delta y}$ at different x/D_e locations). Results in [21] at $x/D_e = 2$ for different cases (dashed line: flapping jet, full line: nonflapping jet) are plotted for comparison. (Color online)

Phase averages retain the intra-cycle dynamics but mask the inter-cycle variability. The fluid dynamical inter-cycle variability can be quantified comparing the kinetic energy density e_φ of the phase averages with the energy density e'_φ of the variances associated to the respective phase averages. This is shown in Fig 11, with e_φ defined as $\rho/(2N_{grid}) \sum_i |V_\varphi|^2$, and e'_φ defined as $\rho/(2N_{grid}) \sum_i var_\varphi(|v|)$. Here, i sweeps the grid points and N_{grid} denotes the number of points in the grid. Parameter e'_φ encompasses different sources of variability including turbulent flucuations, jet flapping, asymmetric flow separation, etc. The comparison between e'_φ and e_φ shows that the phase averages are statistically sound to characterize the flow dynamics. Parameter e'_φ can also be used to check the convergence of the phase averages with respect to the number of samples: computations on 750 and on 1000 images lead to differences on the phase averaged kinetic energy along phases below 3%.

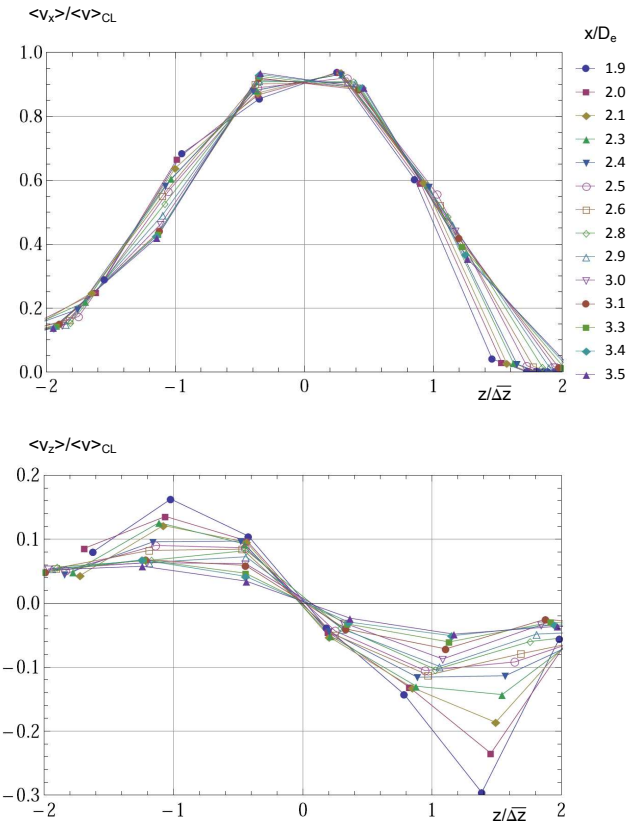

Fig. 10: Normalized mean velocity profiles $\langle v_x \rangle$ and $\langle v_z \rangle$ in the mid-sagittal plane (dependence on $z/\overline{\Delta z}$ at different x/D_e locations). Results in [21] are in these planes are not available. (Color online)

Fig 12 presents a space-time plot of the absolute value of the phase averaged velocity field $V_\varphi(x, y, z)$ along the line $(x, y, z) = (6\ mm, y, 0)$. In the φ range $0 - 270°$, the jet width increases and decreases almost linearly. The flow dynamics replicates the dynamics of a valve exhibiting regular oscillations at $z = 0$ (the glottal width) with an open phase that corresponds to an open quotient of about 0.75. A volumetric characterization of the residual flow observed during complete glottal closure is presented in the following section.

3.3 Three-dimensional Reconstruction

This section presents volumetric reconstructions from phase-averaged velocity fields in the whole field of view. These reconstructions are particularly useful to show in which manner the geometry of the jet changes in space and time.

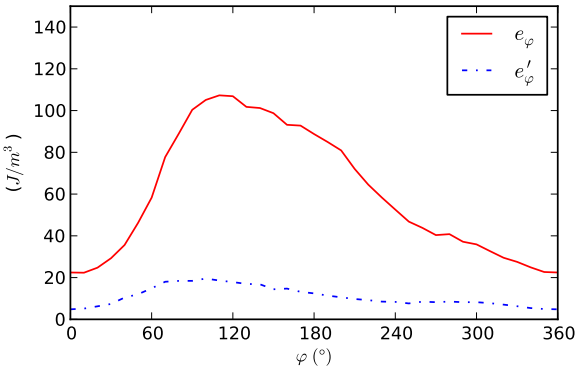

Fig. 11: Inter-cycle variability of the flow, quantified through a comparison of the kinetic energy density of the phase averages (e_φ) and the energy density of the variances associated to them (e'_φ). (Color online)

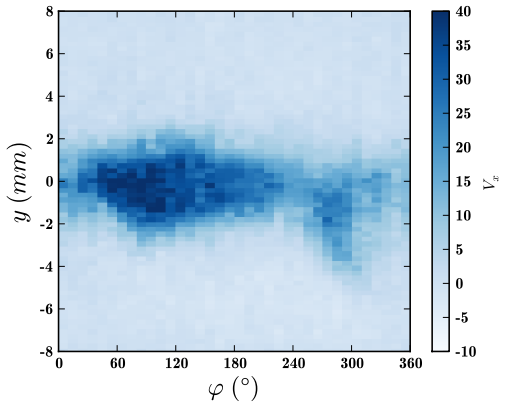

Fig. 12: Space-time plot showing the absolute value of the phase averaged velocity $|V| = |V_\varphi(x, y, z)|$ along the line $(x, y, z) = (6, y, 0)$ mm as a function of the phase φ with a vocal tract attached. (Color online)

Fig 13 shows a reconstruction of the jet based on the streamwise velocity component. In (a) three columns of four streamwise locations are shown. The four streamwise locations are chosen to illustrate the four typical shapes of the cross-section adopted by an axis-switching jet: an elongated shape in the direction of the major axis of the nozzle near the nozzle (two first rows), a diamond-like shape at an intermediate streamwise location (third row), and an elongated shape in the direction of the minor axis of the nozzle further downstream (fourth row). The columns correspond to different data sets. The right column reproduces the four prototypical contours shown in the review by

[11] on non-circular jets. The left and central columns illustrate the four stages for the current data. Notice that four stages of the left and central columns need not occur at the same values of x/D_e as those of the right column. The data in the central column correspond to the a reconstruction of the jet from time averages, while the data on the left column correspond to a reconstruction of the jet at a certain phase ($\varphi \sim 190°$), which has been arbitrarily chosen for illustration purposes. For this same phase, Fig 13(b) shows the volumetric reconstruction that results using the isostreamwise velocity surface of the jet. The vocal tract, which is present in the experiment, is not displayed in the figure for the sake of clarity. The temporal dynamics of this phenomenon is discussed in section 3.4.

The intra-cycle evolution of the jet is shown in Fig 14, through a sequence of representative phases for a volumetric reconstruction using the norm of the phase-averaged velocity fields. Three stages can be noted. The first stage, corresponding to jet formation and fold opening, is represented by the plot with $\varphi = 0°$. During the second stage, illustrated by $\varphi = 40°$ up to $240°$, the volumetric reconstruction shows a jet axis switching occurring at different streamwise positions. In the last two frames, $\varphi = 280°$ and $\varphi = 320°$, the valve is closed but a residual flow is still present. Axis switching leaves its mark in the orientation of the residual flow, which is switched with respect to the major axis of the glottal slit. This is in agreement with the observation of the last quarter cycle of the space-time plot of Fig 12.

3.4 Jet axis switching dynamics

Information on the intra-cycle dynamics of the location of jet axis switching can be extracted from a determination of the jet axis switching crossover distance, defined as the streamwise coordinate x_c where the jet's dimensions at the two axis y and z are equal. The time variation of the jet half widths in the y and z directions along the x-axis is available from the phase averaged fields obtained in the SPIV experiment. Note that $\overline{\Delta y}$ and $\overline{\Delta z}$ presented in section 3.2.2 are computed from time averages, and that a similar computation can be done to obtain Δy and Δz from the phase averages. The region below $x_c/D_e \sim 1.5$ is out of the field of view of the SPIV experiment.

Fig 15(a) shows how the Δy and Δz curves intersect at a certain $x = x_c$ for an arbitrary value of φ lying within the second stage of the flow development. The time-evolution of the half-width of the jet at the crossover distance throughout a glottal cycle is plotted against φ in Fig 15(b), followed by the intra-cycle evolution of the normalized crossover distance x_c in Fig 15(c). The error in these plots is lower than 5%. The size of the jet at the crossover distance gives an indication of the level of contraction/expansion of the jet in the major/minor axis. The crossover distance is found to rise downstream towards a first step around $\varphi \sim 60°$ and then towards a second step around $\varphi \sim 180°$. Before the folds close completely ($\varphi \sim 270°$) the crossover distance decays, and the switching position moves upstream.

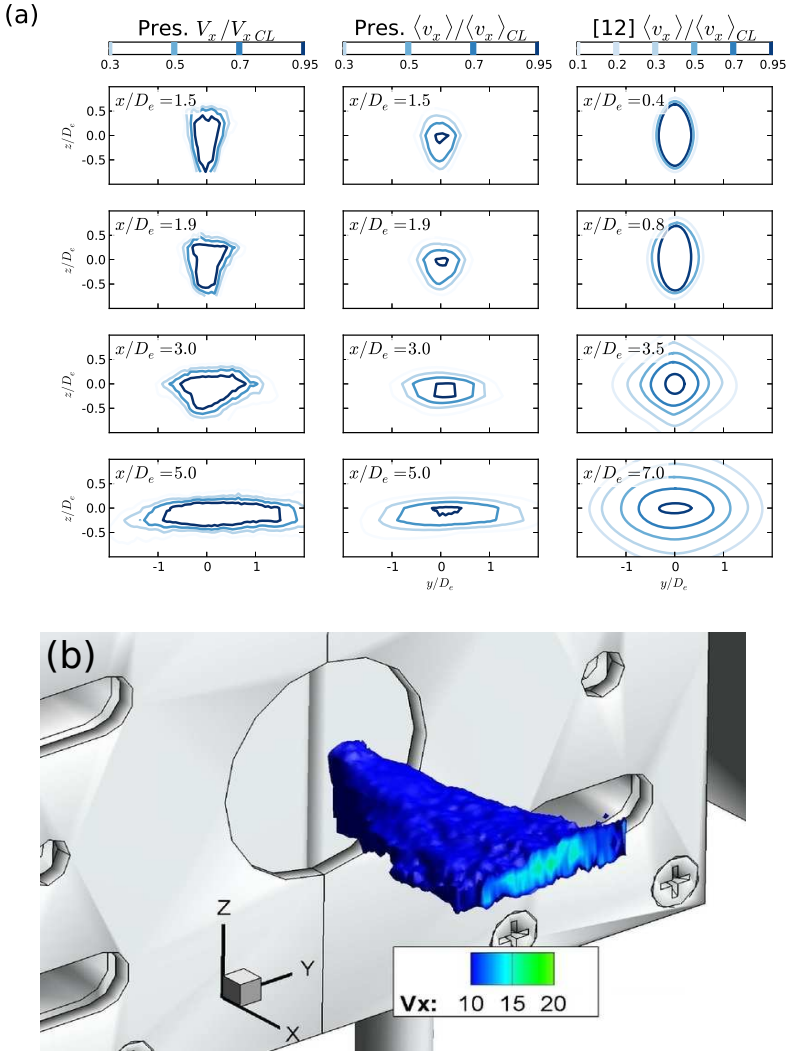

Fig. 13: Jet axis switching in the streamwise velocity fields. (a) Contours illustrating the four typical shapes of the cross-section adopted by an axis-switching jet: Right → elliptic jet in [12] shown as prototypical in [11]. Center → present study, using the time averaged streamwise velocity. Left → present study, using the phase-averaged streamwise velocity for an arbitrary phase ($\varphi = 190°$) within the open phase of the cycle. (b) Volumetric reconstruction using isocontours for V_x in the left column. (Velocity units are m/s). (Color online)

From Gutmark's review on non circular jets [11], mean exit velocity and jet aspect ratio have an influence, among other parameters, upon the axis switching position: the larger the nozzle aspect ratio or the mean exit velocity, the

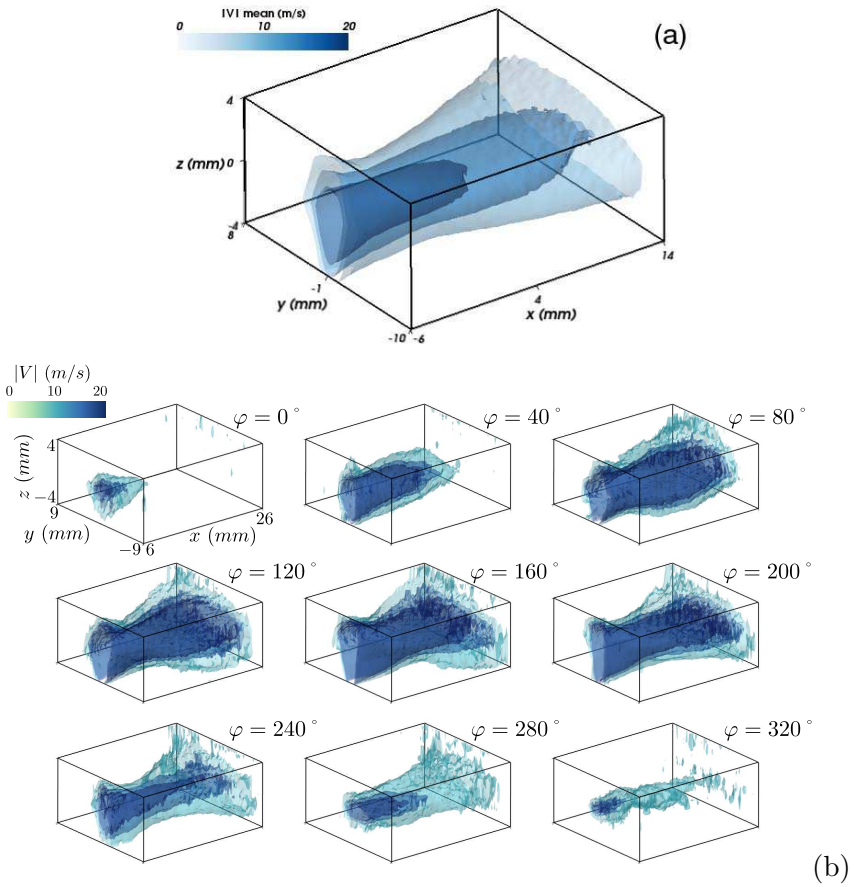

Fig. 14: Absolute value of the time averaged (a) and of the phase averaged (b) flow velocities $|V|$. In (b) phase values are indicated with φ. Three contours are shown, namely, 10, 15 and 20 m/s. The axis box is not coincident with the vocal tract. An animation with the full sequence is available as supplementary material. (Color online)

larger the value of x_c/D_e. The 'nozzle' of this study has a three-dimensional-shape dependency on fold motion which renders determination of the aspect ratio of the jet at the folds quite difficult. A remark is therefore necessary about the aspect ratio of the glottal jet, which involves a distinction between geometrical and fluid dynamical variables. The aspect ratio of the aperture defined by the oscillating folds is geometrical in nature, but the aspect ratio of the jet when it separates from the folds is fluid dynamical. Both aspect ratios are not necessarily coincident, simply because flow separation needs not occur along the glottal neck (*i.e.* there where the glottal width is narrowest). Numerical studies have shown that, in general, the width of the glottal jet cannot be

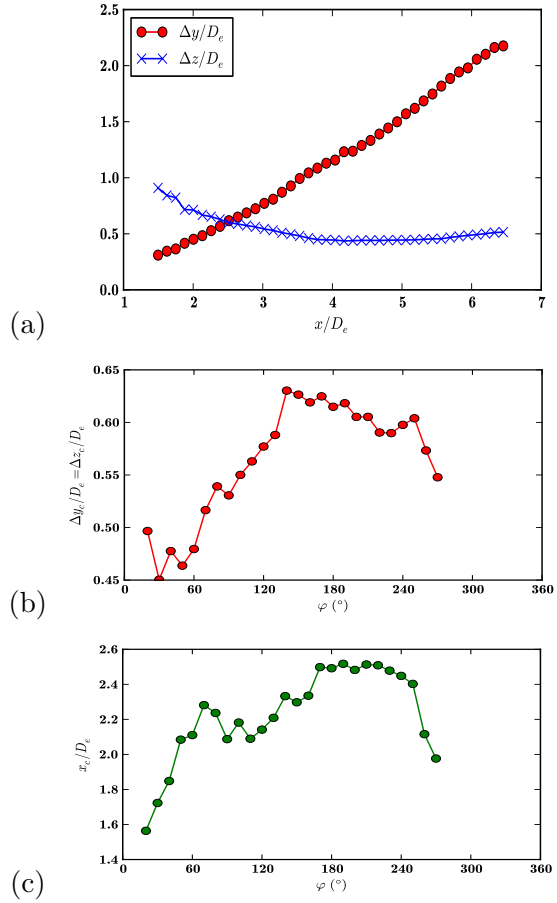

Fig. 15: Characterization of jet axis switching dynamics. (a) Jet half widths ($\Delta y/D_e$, $\Delta z/D_e$) as a function of normalized downstream distance (x/D_e) for $\varphi = 200°$ with crossing at x_c/D_e. (b) Intra-cycle evolution of the jet half-width at the crossover distance. (c) Crossover distance x_c/D_e versus φ (color online).

reduced to a geometrical function of wall motion [29]. In other words, glottal jet exit contour cannot be recovered from glottal exit geometry.

In this vocal fold model, flow separation must occur along a line defining the jet exit contour as the folds oscillate, and this separation line needs not even lie on a single transverse plane, since fold motion is three-dimensional. Nevertheless, an indication of the time-variation of jet aspect ratio at the valve exit can be extracted from the aspect ratio of the jet at the transverse plane closest to the flow discharge. Jet aspect ratio at this plane is condensing the information on jet separation occurred immediately upstream. Fig 16(a) shows the evolution of the ratio ($\Delta z/\Delta y$) at this plane. This ratio follows the same

trends of the crossover distance dynamics $x_c(\varphi)$: it rises towards a first step around $\varphi \sim 60°$ and then towards a second step around $\varphi \sim 180°$, attaining the lowest values for the φ ranges where $x_c/D_e < 2$. Notice that the flow rate, shown in Fig 16(b), has a different waveform. It can therefore be retained that the jet aspect ratio dynamics seems to play an important role in determining the crossover position $x_c(t)$.

Flow separation is known to affect the driving force determining vocal fold motion and is therefore an important issue in voice production modelling. If $x_c(\varphi)$ is correlated with flow separation at the jet exit, as these results suggest, the switch position of the glottal jet can become an important magnitude in glottal jet studies.

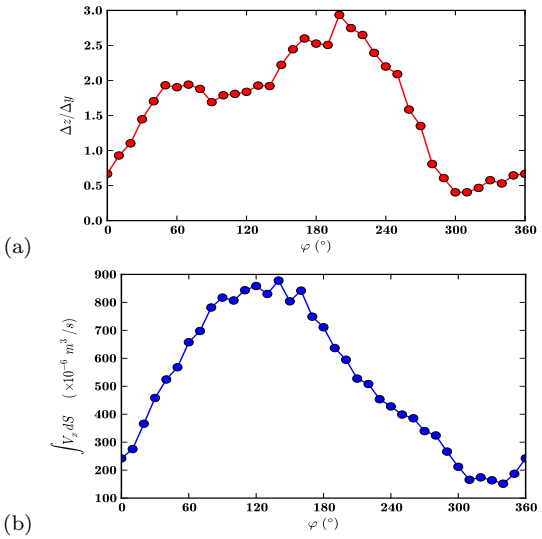

Fig. 16: Intra-cycle evolution of the phase averages at the transverse plane closest to the glottis ($x \sim 6$ mm). (a) Jet aspect ratio ($\Delta z/\Delta y$) and (b) Streamwise velocity surface integral over the measurement section ($\int V_x dS$).

4 Concluding remarks

This work investigates the airflow produced by a life-size model mimicking vocal fold motion in many important aspects: self-sustained oscillations are attained within a fluid-structure-acoustic interaction process, the glottal outlet adopts an elongated time-varying shape with corners at the commisures, a tonal sound is generated in the far field of the experimental setup, and the sound pitch, which can be controlled through the variation of the natural frequency of the structure, has a non zero jitter. The pulsating jet generated

with this model is confined by the presence of a uniform vocal tract having a life-size length.

Previous glottal jet studies had stressed the three-dimensional nature of this complex biological flow from results obtained with 2D-PIV techniques. In this work, a three-dimensional characterization of this flow is proposed, using a 3D-PIV technique (SPIV) and a post-synchronisation method of the velocity fields based on the audio signal generated by the pulsating jet. The flow analysis contains three novel features: a documentation of the time-averaged flow properties along the minor and major axes of the glottal jet, a volumetric reconstruction from phase averaged velocity fields, and a space-time account of the most prominent three-dimensional effect. This characterization is performed for a flow region confined by the lateral walls of the vocal tract, within a volume lying as close as possible to the oscillating folds.

Time-averaged flow fields do not allow for an interpretation in terms of a mean field subject to small perturbations, since glottal flow is a highly unsteady interrupted flow through a closing valve, but they have the interesting property of bearing the signature of the three-dimensionality of the flow. This can be appreciated both, in the reconstructed mean velocity field, and in the variation of jet spread in the mid-sagittal plane, which successively contracts and expands in the inspected region. This behavior of the mean jet spread in the major axis has been reported for axis switching steady jets in studies using non-circular nozzle. On the other hand, the mean jet spread in the mid-coronal plane compares well with the nonflapping jet characterized in a recent study using a self-oscillating flexible nozzle [21]. Documentation of the mean velocity profiles shows a good collapse of the streamwise velocity, and a shape-preserving waveform for the spanwise velocity in the minor an major axes. This finding suggests that a similarity analysis of these profiles, reproducing those conducted for synthetic jets, might lead to interesting results.

Glottal jet studies prior to this characterization had signalled the existence of jet axis switching inferring the switch from the mid-sagittal narrowing of the jet flow. The volumetric reconstruction presented in the present work provides further insight into this phenomenon. It shows that the switch does not occur at a fixed distance from the folds during the glottal cycle. In fact, the switch occurs farthest from the valve exit region towards the second part of the open phase of the cycle. During closure, it is found that the switching leaves its mark on the orientation of the residual flow, which is found to be perpendicular to the contact line between the folds.

An analysis of the switching dynamics is presented in terms of the downstream location at which the switch occurs. The rapid contraction/expansion of the jet in the major/minor axis is quantified through the size of the jet at this location. This magnitude gives a measure of the high three-dimensionality of the laterally confined jet within a flow volume lying significantly close to the valve exit. For non-pulsating jets exiting elongated nozzles, the location at which the switch occurs, referred to as the crossover distance, is sensitive to a number of parameters which includes nozzle aspect ratio. The aspect ratio of the jet studied in this work depends on flow separation from the self-

oscillating folds. The intra-cycle evolution of the crossover distance is found to be similar to the time-variation of the aspect ratio of the jet in the transverse plane closest to the flow discharge. This finding is in line with the reported dependence of the switch position with nozzle aspect ratio for steady jets. If this dependence effectively governs the switch of the glottal jet, the crossover distance becomes an interesting magnitude, bearing the space-time signature of flow separation at the moving folds.

This flow analysis provides a three-dimensional portrait of the flow generated by a particular vocal fold model. Naturally, the relevant parameters invoked in non-circular jet characterization (volume flow velocity, aspect ratio, inlet geometry) associate conveniently to sustain fold motion in this model and cannot be tuned independently. Three-dimensional jet studies in configurations allowing to consider the separate influence of these parameters should help provide a more general picture of this kind of confined pulsating flow.

Acknowledgements This research has been performed with the support of the SticAmSud Program 'Modelling Voice Production', of the Bernardo Houssay Program and of the LIA PMF-FMF (Franco-Argentinian International Associated Laboratory in the Physics and Mechanics of Fluids). We wish to acknowledge the generosity of X. Pelorson concerning the experimental design of the vocal fold model.

References

1. Agrawal, A., Verma, G.: Similarity analysis of planar and axisymmetric turbulent synthetic jets. International Journal of Heat and Mass Transfer **51**, 6194–6198 (2011)
2. Becker, S., Kniesburges, S., Muller, S., Delgado, A., Link, G., Kaltenbacher, M., Dollinger, M.: Flow-structure-acoustic interaction in a human voice model. J. Acoust. Soc. Am. **125 (3)**, 1351 (2009)
3. Boersma, P., Weenink, D.: Praat, a system for doing phonetics by computer. Glot. International **5**, 341–345 (2001)
4. Cheing, R., Chung, J.N.: Simulation of particle dispersion in a two dimensional mixing layer. AIChE J. **34**, 946 (1988)
5. Chisari, N.E., Artana, G., Sciamarella, D.: Vortex dipolar structures in a rigid model of the larynx at flow onset. Exp. Fluids **50**, 397–406 (2011)
6. Drechsel, J.S., Thomson, S.L.: Influence of supraglottal structures on the glottal jet exiting a two-layer synthetic, self-oscillating vocal fold model. J. Acoust. Soc. Am. **123 (6)**, 4434–4445 (2008)
7. Erath, B.D., Plesniak, M.W.: An investigation of asymmetric flow features in a scaled-up driven model of the human vocal folds. Exp. Fluids **49 (1)**, 131–146 (2010)
8. Erath, B.D., Plesniak, M.W.: Impact of wall rotation on supraglottal jet stability in voiced speech. J. Acoust. Soc. Am. **129 (3)**, EL64–EL70 (2011)
9. Fuchs, N.A.: The mechanics of aerosols. Dover Publications. Inc. New York (1964)
10. Gilbert, J., Ponthus, S., Petiot, J.F.: Artificial buzzing lips and brass instruments: Experimental results. J. Acoust. Soc. Am. **104 (3)**, 1627–1632 (1998)
11. Gutmark, E.J., Grinstein, F.F.: Flow control with noncircular jets. Ann. Rev. Fluid Mech. **31**, 239–272 (1999)
12. Ho, C.M., Gutmark, E.: Vortex induction and mass entrainment in a small-aspect-ratio elliptic jet. J. Fluid Mech. **179**, 383–405 (1987)
13. Hollien, H., Dew, D., Philips, P.: Phonational frequency ranges of adults. J. Speech and Hearing Res. **14**, 755–760 (1971)
14. Hussain, F., Husain, H.S.: Elliptic jets. part 1. characteristics of unexcited and excited jets. J. Fluid Mech. **208**, 257–320 (1989)

15. Khosla, S., Muruguppan, S., Gutmark, E., Scherer, R.: Vortical flow field during phonation in an excised canine larynx model. Ann. Otol. Rhinol. Laryngol. **116 (3)**, 217–228 (2007)
16. Khosla, S., Muruguppan, S., Gutmark, E., Scherer, R.: Using particle imaging velocimetry to measure anterior-posterior velocity gradients in the excised canine larynx model. Ann. Otol. Rhinol. Laryngol. **117 (2)**, 134–144 (2008)
17. Konrath, R., Schroder, W.: Stereoscopic particle-image velocimetry (piv) a new approach using telecentric lenses. 10th Int'lSymposium on Applications of Laser Techniques to Fluid Mechanics' pp. 1–14 (2000)
18. Krane, M., Barry, M., Wei, T.: Unsteady behavior of flow in a scaled-up vocal folds model. J. Acoust. Soc. Am. **122 (6)**, 3659–3670 (2007)
19. Krebs, F., Artana, G., Sciamarella, D.: Glottal aperture modes and acoustic output in an in-vitro self-oscillating vocal fold model. 10eme Congrès Français d'Acoustique p. CFA2010/412 (2010)
20. Krothapalli, A., Baganoff, D., Karamcheti, K.: On the mixing of a rectangular jet. J. Fluid Mech. **107**, 201–220 (1981)
21. Murugappan, S., Gutmark, E.J., Lakhamraju, R.R., Khosla, S.: Flow-structure interaction effects on a jet emanating from a flexible nozzle. Phys. Fluids **20 (11)**, 117,105 (2008)
22. Neubauer, J., Zhang, Z., Miraghaie, R., Berry, D.A.: Coherent structures of the near field flow in a self-oscillating physical model of the vocal folds. J. Acoust. Soc. Am. **121 (2)**, 1102–1118 (2007)
23. Pelorson, X., Hirschberg, A., Hasselt, R.V., Wijnands, A., Auregan, Y.: Theoretical and experimental study of quasisteady-flow separation within the glottis during phonation.Application to a modified two-mass model. J. Acoust. Soc. Am. **96 (6)**, 3416–3431 (1994)
24. Prasad, A.K.: Stereoscopic particle image velocimetry. Exp. Fluids **29**, 103–116 (2000)
25. Quinn, W.R.: Experimental study of the near field and transition region of a free jet issuing from a sharp-edged elliptic orifice plate. European journal of Mechanics - B/Fluids **26**, 583–614 (2007)
26. Raffel, M., Willert, C.E., Kompenhans, J.: Particle Image Velocimetry. A Practical Guide. Springer-Verlag Berlin Heidelberg (1998)
27. Ruty, N., Pelorson, X., Hirtum, A.V.: Influence of acoustic waveguides lengths on self-sustained oscillations: Theoretical prediction and experimental validation. J. Acoust. Soc. Am. **123 (5)**, 3121 (2008)
28. Ruty, N., Pelorson, X., Hirtum, A.V., Lopez-Arteaga, I., Hirschberg, A.: An in vitro setup to test the relevance and the accuracy of low-order vocal folds models. J. Acoust. Soc. Am. **121 (1)**, 479–490 (2007)
29. Sciamarella, D., Quéré, P.L.: Solving for unsteady airflow in a glottal model with immersed moving boundaries. European journal of Mechanics - B/Fluids **27(1)**, 42–53 (2008)
30. Sidlof, P., Doare, O., Cadot, O., Chaigne, A.: Measurement of flow separation in a human vocal folds model. Exp. Fluids **51**, 123–136 (2011)
31. Svec, J.G., Horacek, J., Sram, F., Vesely, J.: Resonance properties of the vocal folds: In vivo laryngoscopic investigation of the externally excited laryngeal vibrations. J. Acoust. Soc. Am. **108 (4)**, 1397 (2000)
32. Titze, I.R., Liang, H.: Comparison of high precision f0 extraction algorithms for sustained vowels. J. Speech and Hearing Res. **36**, 1120–1133 (1993)
33. Triep, M., Brucker, C.: Three-dimensional nature of the glottal jet. J. Acoust. Soc. Am. **127 (3)**, 1537–1547 (2010)
34. Triep, M., Brucker, C., Schroder, W.: High-speed piv measurements of the flow downstream of a dynamic mechanical model of the human vocal folds. Exp. Fluids **39**, 232–245 (2005)
35. Vilain, C.E., Pelorson, X., Hirschberg, A., Marrec, L.L., Root, W.O., Willems, J.: Contribution to the physical modeling of the lips. influence of the mechanical boundary conditions. Acta Acustica united with Acustica **89**, 882–887 (2003)
36. Yoon, J.H., Lee, S.J.: Investigation of the near-field structure of an elliptic jet using stereoscopic particle image velocimetry. Meas. Sci. Technol. **14**, 2034–2046 (2003)
37. Zhang, Z., Neubauer, J.: On the acoustical relevance of supraglottal flow structures to low-frequency voice production. J. Acoust. Soc. Am. **128 (6)**, EL378–EL383 (2010)